Theoretical Evaluation of Energy, Exergy, and Minimum Superheat in a High-Temperature Heat Pump with Low GWP Refrigerants

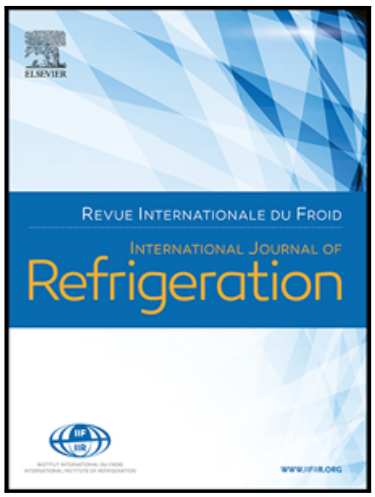

Theoretical Evaluation of Energy, Exergy, and Minimum Superheat in a High-Temperature Heat Pump with Low GWP Refrigerants{fr}Évaluation théorique de l'énergie, de l'exergie et de la surchauffe minimale dans une pompe à chaleur à haute température avec des réfrigérants à faible GWP

Adam Y. Sulaiman , Donal Cotter , Cordin Arpagaus , Neil Hewitt

PII: S0140-7007(23)00150-0
DOI: https://doi.org/10.1016/j.ijrefrig.2023.06.001
Reference: JIJR 5878

To appear in: *International Journal of Refrigeration*

Received date: 14 February 2023
Revised date: 31 May 2023
Accepted date: 1 June 2023

Please cite this article as: Adam Y. Sulaiman , Donal Cotter , Cordin Arpagaus , Neil Hewitt , Theoretical Evaluation of Energy, Exergy, and Minimum Superheat in a High-Temperature Heat Pump with Low GWP Refrigerants{fr}Évaluation théorique de l'énergie, de l'exergie et de la surchauffe minimale dans une pompe à chaleur à haute température avec des réfrigérants à faible GWP, *International Journal of Refrigeration* (2023), doi: https://doi.org/10.1016/j.ijrefrig.2023.06.001

Highlights

- The environmental and thermophysical characteristics of the investigated working fluids were comprehensively evaluated.
- The research focuses on mapping the minimum superheat for various selected refrigerants.
- The favourable impact of mapping the minimum superheat on both energetic and exergetic performance.
- The potential replacements for HFC-245fa and HFC-365mfc are HCFO-1233zd(E) and HFO-1336mzz(Z), respectively.

Theoretical Evaluation of Energy, Exergy, and Minimum Superheat in a High-Temperature Heat Pump with Low GWP Refrigerants

Adam Y. Sulaiman[1*], Donal Cotter[1], Cordin Arpagaus[2], Neil Hewitt[1]

[(1)]Centre for Sustainable Technologies, Belfast School of Architecture and The Built Environment, Ulster University, 2-51 York Street, Belfast, Co. Antrim, BT15 1ED, UK
sulaiman-w@ulster.ac.uk

[(2)]Eastern Switzerland University of Applied Sciences, Institute for Energy Systems, Werdenbergstrasse 4, CH-9471 Buchs, Switzerland
cordin.arpagaus@ost.ch

*Corresponding author

French title

Évaluation théorique de l'énergie, de l'exergie et de la surchauffe minimale dans une pompe à chaleur à haute température avec des réfrigérants à faible GWP

Mots-clés : Pompe à chaleur haute température, surchauffe minimale, Efficacité énergétique et exergétique, Fluides frigorigènes à faible GWP.

Abstract

Suitable low global warming potential (GWP) refrigerants that conform to F-gas regulations are fundamental to the operation and future development of high-temperature heat pumps (HTHPs) used for industrial processes and waste heat recovery. This paper presents the results of a theoretical simulation to investigate a range of low-GWP refrigerants and their suitability to supersede refrigerants HFC-245fa and HFC-365mfc. A steady-state thermodynamic model of a single-stage HTHP with an internal heat exchanger (IHX) was developed to assess system cycle characteristics and performance at temperature setpoints at 60 and 70 °C heat source, 90 and 140 °C heat sink, at 30 and 70 K lift. This study focuses on energetic and exergetic efficiencies within the system and the impact of regulating superheat to optimise performance. Based on energetic and exergetic theoretical results, a trade-off between COP, VHC, and exergetic efficiency indicates HCFO-1233zd(E) and HFO-1336mzz(Z) as the most likely replacements for HFC-245fa and HFC-365mfc respectively. The refrigerant HC-601, followed by HFO-1336mzz(Z) and HCFO-1233zd(E), exhibited the lowest exergetic destruction within test conditions. Mapping the minimum superheat indicated optimum performance for HCFO-1233zd(E) between 5 to 8 K and HFO-1336mzz(Z) between 17 to 22 K, depending on temperature lift. Validation of the theoretical results with experimental data indicates

that simulated COP closely matches empirical values. This work provides a method to optimise refrigerant selection in HTHPs based on operational indicators to maximise overall system performance.

Keywords: High-temperature heat pump, minimum superheat, Energy & exergy efficiency, Low GWP refrigerants.

Nomenclatures

COP	coefficient of performance (-)
F	factor (-)
h	specific enthalpy (kJ kg^{-1})
P	pressure (bar)
s	specific entropy (kJ kg^{-1} K^{-1})
T	temperature (°C)
VHC	volumetric heat capacity (kJ m^{-3})

Abbreviations

GWP	global warming potential
HP	heat pump
HTHP	high-temperature heat pump
HCFO	hydrochlorofluoroolefin
HFC	hydrofluorocarbons
HFO	hydrofluoroolefin
IHX	internal heat exchanger
NBP	normal boiling point
ODP	ozone depletion potential
PR	pressure ratio
TEWI	total equivalent warming impact

Subscript

adj	adjustable
comp	compressor
Cond	condenser
Crit	critical
Dest	destruction
Ex	exergy
Evap	evaporator
Exp	electronic expansion valve
Lift	temperature lift
Min	minimum
OH	overhanging
SH	superheat
Sink	heat sink
source	heat source
Suc	suction
Theo	theoretical
Vol	volumetric

Greek symbols

E	effectiveness (-)
f	function (-)
Ƞ	efficiency (-)
Δ	variation

1. Introduction

There has been dramatic growth in the world's economy over the last decade, resulting in a significant increase within the industrial sector and a subsequent rise in primary energy consumption and CO_2 emissions. Furthermore, a considerable amount of energy is wasted within industrial processes as waste heat, leading to significant losses (Worrella & Biermans, 2005). The term "industrial waste heat" refers to the dissipation and loss of heat during production processes utilising energy (typically electricity and heat) to manufacture products. The literature demonstrates that 72% of the world's primary energy supply is dissipated through these conversion processes (Bianchi, et al., 2019). The industrial sector uses approximately 22% primary energy while releasing over 50% to the atmosphere as waste heat. Due to technical and economic constraints, roughly 3.8% of the world's main energy consumption in 2019 was released as low-grade waste heat from industrial activity at temperatures below 100 °C (Forman, et al., 2016). According to 2019 data estimated by Odyssee-Mure (2019), the EU 28 (including the UK) final energy consumption was approximately 946.5 Mtoe (11005.5 TWh), as shown in Fig. 1, representing nearly 10% of the world's total final energy consumption (IEA, 2022). This resulted in CO_2 emissions of about 4074 $MMTCO_2$-Eq, corresponding to about 12% of the world's CO_2 emissions (Statista GmbH, 2022). Moreover, the industrial sector in the EU

consumed approximately 2989 TWh in 2019, representing 27.2% of the total energy consumption and contributing to about 21.6% of the EU's final CO_2 emissions (EEA, 2021).

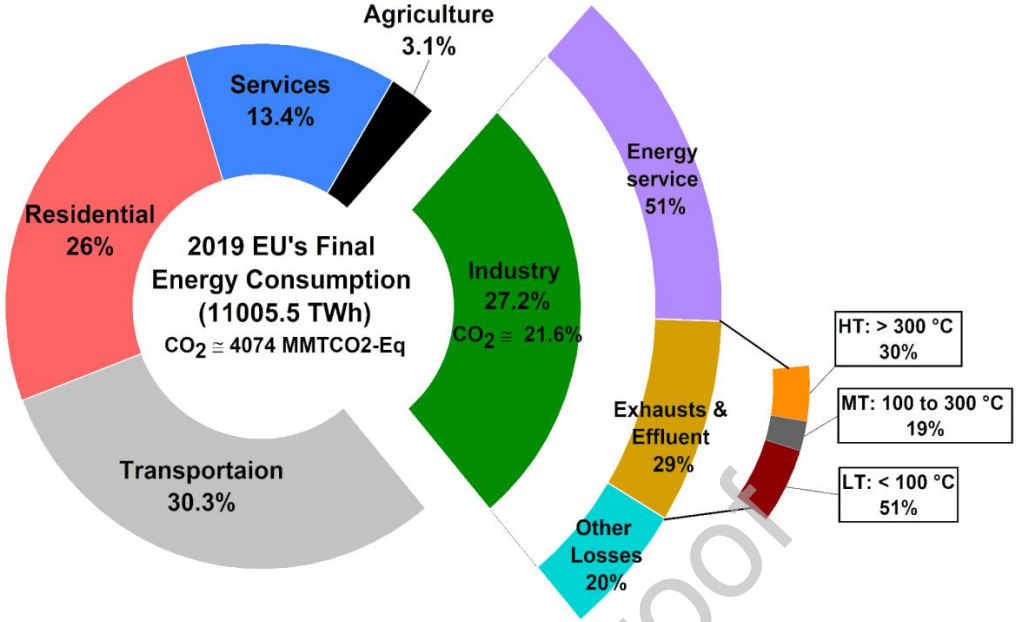

Fig. 1. Final energy consumption (2019) within the EU 28. The industrial sector is expanded to show estimated waste heat potential occurring within different temperature ranges (LT: <100 °C, MT: 100 to 300 °C, HT: >300 °C) (Data source: (Bianchi, et al., 2019; Forman, et al., 2016)).

Thermodynamics describes energy as the aggregate of exergy and anergy, wherein exergy is the energy that may be converted into mechanical work, and anergy is the exergy that is destroyed during the conversion process (Mujahid Rafique, et al., 2016). The data indicates that nearly 867 TWh (approximately 29% of industrial consumption) was converted to anergy in the form of exhaust or effluents. The waste heat recovery potential can be further subdivided according to temperature ranges, typically classified as "low" (LT): <100 °C, "medium" (MT): 100 to 300 °C, and "high" (HT): >300 °C (Bianchi, et al., 2019; Forman, et al., 2016), as shown in Fig. 1. The waste heat at low temperatures constitutes more than 51% of the overall waste heat from exhaust and effluent, which is around 442 TWh (≅ 4% of the EU's total energy consumption) (Papapetrou, et al., 2016).

With a significant amount (70%) of the industrial sector's surplus heat falling into the LT and MT categories, upgrading this surplus heat can boost energy efficiency and support the decarbonisation challenge within this sector. Employing a thermodynamic cycle and external input power, the working fluid that gains enthalpy throughout the heat recovery process undergoes a sequence of thermodynamic conversions providing a positive energy output (Ommen, et al., 2015).

Electrically driven high-temperature heat pumps (HTHP) could offer a practical solution in many sectors to improve energy efficiency and decarbonise energy-intensive industrial processes. The HTHP technology can be integrated within many industrial applications to reprocess low-temperature waste heat (LT part shown in Fig. 1) and upgrade it to useful heat up to about 165 °C (Arpagaus, et al., 2018). Increasing the operational envelope of this technology to achieve higher sink outlet temperatures up to 200 °C would greatly increase the potential suitability in a wider range of industrial processes (e.g., drying processes and steam generation) (Arpagaus, et al., 2020; IEA HPT, 2023). The development of HTHPs to achieve high sink temperatures greatly depends on the available waste heat temperature, temperature lift, working fluid selection, and heat pump cycle configuration. Many research studies predominantly used single-stage cycles incorporating an internal heat exchanger (IHX) to assess system performance with low GWP refrigerant types (Arpagaus, et al.,

2018). Some HTHP experimental studies have investigated hydrochlorofluoroolefins (HCFOs) and hydrofluoroolefins (HFOs) refrigerant types HCFO-1224yd(Z), HCFO-1233zd(E), HFO-1336mzz(Z) (Mateu-Royo, et al., 2019; Arpagaus & Bertsch, 2019), and natural refrigerant HC-600 (n-butane) (Bamigbetan, et al., 2019). Alongside energetic evaluation, exergetic analysis is crucial to analyse the HTHP quality of the process and determine the losses associated with each component. Some experimental studies have completed energy and exergy analyses to assess the technology's overall performance (Arpagaus, et al., 2018; Mateu-Royo, et al., 2019).

Theoretical simulation of different HTHP cycle configurations provides a method to model many different refrigerant types to assess performance. Arpagaus & Bertsch, (2020) investigated HFO-1336mzz(Z), HCFO-1233zd(E) and HCFO-1224yd(Z), comparing the coefficient of performance (COP) and volumetric heating capacity (VHC) with HFC-245fa and HFC-365mfc. Bamigbetan et al. (2018) used theoretical modelling to assess natural refrigerants like hydrocarbons (HC), and synthetic hydrofluorocarbons (HFC), HFOs, and HCFOs, identifying HC-600 and HCFO-1233zd(E) as potential candidates in HTHPs. Mikielewicz & Wajs (2019) evaluated the theoretical exergetic efficiency and exergy destruction of a single-stage and cascade type of HTHP using low GWP refrigerants. In a single-stage HTHP system, ethanol (no ASHRAE class) and HC-601 (n-pentane) showed the best exergetic efficiency and the lowest exergetic destruction. Mateu-Royo et al. (2019) experimentally analysed the exergetic efficiency in a single-stage HTHP system using the exergy balances for each component, identifying the compressor and expansion valve with the highest potential for efficiency improvement. Finally, a recent paper by Sulaiman et al. (2022) theoretically compared low-GWP refrigerants as a potential substitute for R245fa based on their environmental and thermodynamic characteristics.

This paper investigates a range of various HFOs, HCFOs, and HCs to determine the most suitable candidates to replace HFC-245fa and HFC-365mfc in HTHP applications. First, a general theoretical study by Sulaiman et al. (2022) was further developed to assess HTHP cycle performance based on energy and exergy analysis to evaluate various areas, including minimum superheat, heat transfer and the total equivalent warming impact (TEWI). Based on these theoretical simulations, an in-depth practical method to estimate refrigerant operational performance was developed that may be useful to advance HTHP systems. Furthermore, this study thoroughly investigated how to graphically characterise mapping the minimum superheat required by the compressor for various promising low GWP working fluids, highlighting their impact on energetic and exergetic performance. In addition, the model validation was performed to evaluate the simulation's accuracy based on refrigerants HCFO-1224yd(Z), HCFO-1233zd(E), and HFO-1336mzz(Z). Finally, experimental results from Arpagaus & Bertsch, (2019) of a single-stage HTHP with IHX were used for comparison.

2. Refrigerant screening

The introduction of F-gas regulations and planned phase-down of high GWP refrigerants require the developing, testing, and availability of suitable commercial replacement working fluids (ASHRAE, 2022; DEFRA, 2022). In HTHPs, refrigerant selection plays a major role in optimum cycle design, predicting the level of discharge temperature, mapping the energetic and exergetic efficiency, and selecting components (Arpagaus, et al., 2018). Table 1 presents the thermophysical and environmental properties of selected refrigerants suitable for HTHP applications. Values for T_{crit}: Critical temperature, P_{crit}: Critical pressure & NBP: Normal boiling point (NIST, 2018). ODP: Ozone depletion potential (UNEP, 2020), GWP_{100yrs}: Global warming potential 100 years (UNEP, 2020; Myhre, et al., 2013; EUR-Lex, 2014). SG: Safety Group classification (ASHRAE, 2022). Additional details; AMOLEA™ 1224yd: (AMOLEA, 2023), Honeywell Solstice®zd (Honeywell , 2023), SOLKANE®365mfc (SOLKANE, 2023), HFO-1234ze(Z): Fukuda, et al., (2014) (not commercially available), Opteon™ SF33 or Opteon™ MZ (HFO-1336mzz-Z) (Opteon, 2023). Phase down of HFC-245fa and HFC-365mfc with GWP >150 (Shaded). Cp/Cv: calculated at atmospheric pressure 1.013 bar at 25 °C.

Since HTHP systems operate at high pressures and temperatures, the refrigerant safety classification plays a crucial role in the unit's designation and installation (ASHRAE, 2022). ASHRAE provides refrigerants ratings and safety categories based on the manufacturer-supplied toxicity and flammability data. Refrigerants of class A are less hazardous than those of class B. The umbrella term of flammability includes three categories and one subclass. Class 1 for refrigerants that do not propagate a flame when tested according to the standard; class 2 for refrigerants with reduced flammability; and class 3 for extremely flammable refrigerants, such as hydrocarbons. ASHRAE altered the safety classification matrix to include a new flammability subclass 2L for class 2 refrigerants that flame slowly. A2L HFOs have a moderate global warming potential and are moderately flammable.

Fig. 2. characterises each refrigerant's pressure and temperature ranges as a function of enthalpy, displaying a wide range of variation within the array. These refrigerants currently represent promising replacements for HFC-245fa and HFC-365mfc, which will be phased down to 21% of 2014 sales by 2030 (EUR-Lex, 2014) in line with F-gas legislation in the EU and other developed countries.

Table 1: The thermophysical and environmental characteristics of low-GWP replacements (GWP <150) for HTHPs.

Type	Refrigerant (ASHRAE)	Composition	ODP	GWP_{100yrs}	T_{crit} [°C]	P_{crit} [bar]	Cp/Cv	NBP	SG
HC	R600	C_4H_{10}	0	4	152.01	37.96	1.105	0.0	A3
HC	R601	C_5H_{12}	0	5	196.56	33.58	1.336	36.1	A3
HCFO	R1224yd(Z)	C_3HF_4CI	0.00023	1	156.00	33.30	1.098	14.0	A1
HCFO	R1233zd(E)	$C_3H_2CIF_3$	0.00034	1	166.50	36.20	1.104	18.0	A1
HFC	R245fa	$C_3H_3F_5$	0	**1030**	154.05	36.40	1.101	15.0	B1
HFC	R365mfc	$C_4H_5F_5$	0	**794**	186.85	32.66	1.331	40.0	A2
HFO	R1234ze(Z)	$C_3F_4H_2$	0	<10	150.10	35.30	1.119	9.8	A2L
HFO	R1336mzz(Z)	$C_4H_2F_6$	0	2	171.30	29.00	1.001	33.4	A1

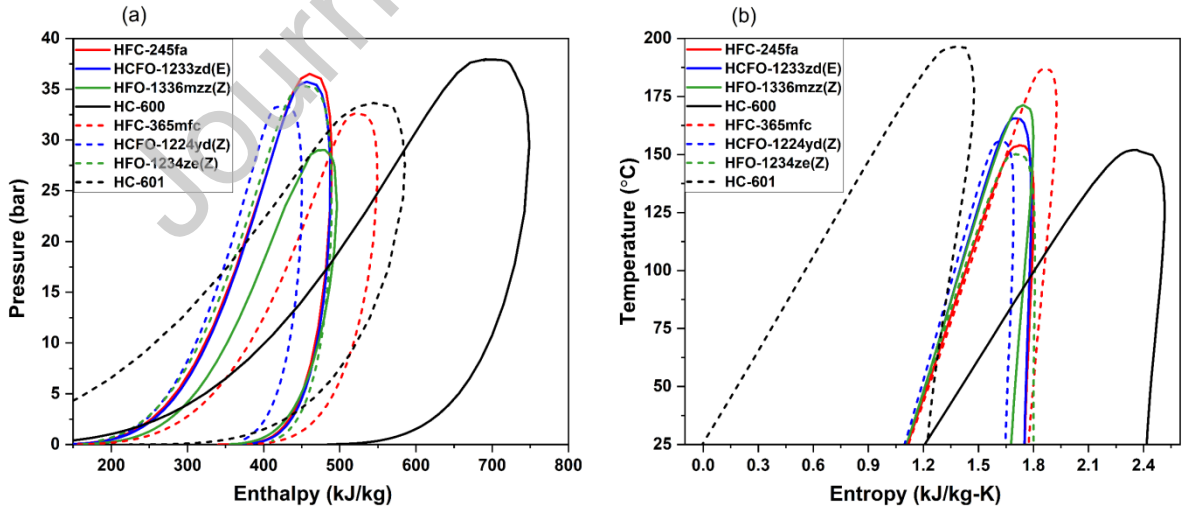

Fig. 2. (a) P-h and (b) T-s diagrams for selected low GWP refrigerants that are potential alternatives to HFC-245fa and HFC-365mfc in HTHP applications (Plotted with data from REFPROP (NIST, 2018)).

The refrigerant HFO-1336mzz(Z) is non-flammable and chemically stable at high temperatures compared to other refrigerants, offering a high critical temperature of 171.3 °C with a normal boiling

point of 33.4 °C (Kontomaris, 2014). The refrigerant HCFO-1233zd(E) has a higher critical temperature than HFC-245fa and offers similar thermodynamic properties and boiling heat transfer (Patten & Wuebbles, 2010). HCFO-1233zd(E) has an ODP value of 0.00034 and a safety group classification of A1. HFO-1234ze(Z) has zero ODP and less than 10 GWP value, and it has a critical temperature and pressure close to HFC-245fa. It has a similar vapour pressure curve and similar thermal conductivities with lower viscosities resulting in better heat transfer (Petr & Raabe, 2015). HCFO-1224yd(Z) has an ODP value of 0.00023 and a short molecular lifetime (20 days), resulting in a low GWP value (Eyerer, et al., 2019). The A1, non-flammable HCFO-1224yd(Z), has a similar critical temperature to HFC-245fa, with lower vapour and critical pressure. It also has a VHC about 8.5% lower than HFC-245fa, operating at similar volumetric flow rates (Mateu-Royo, et al., 2021). The refrigerants HC-600 and HC-601 are hydrocarbons with zero ODP and low GWP. Both are flammable and classified in the A3 safety group; thus, increased safety measures are required for these substances (Besagni, et al., 2015).

Finally, the subject of trifluoroacetic acid (TFA, C2HF3O2) as a potential atmospheric degradation product of some HFC, HFO, and HCFO refrigerants has sparked controversy over the environmental risks and long-term viability of HFO/HCFOs as a new generation of refrigerants. There is widespread agreement that TFA is a strong organic acid that is highly persistent once released into the environment. As a result, the national authorities of Denmark, Germany, the Netherlands, Norway, and Sweden submitted a proposal to the EU chemicals agency ECHA to restrict per- and polyfluoroalkyl substances (PFAS) under REACH, which could include HFO/HCFO refrigerants. The history of HCFC and HFC refrigerants teaches us to be extremely cautious with new synthetic refrigerants. It would therefore be prudent to limit HFOs to applications where suitable alternative refrigerants are not available.

3. Cycle configuration

In this work, theoretical simulations of a HTHP cycle configuration were performed in Engineering Equation Solver (EES) software (Klein, 2017) to assess energy and exergy for the selected refrigerants at various operational conditions. Fig. 3 exhibits the investigated system configuration in addition to the Log P-h and T-s diagrams. The main components within the system are a compressor, condenser, expansion valve, evaporator, and IHX. The IHX is situated between the suction and liquid lines to add the necessary superheat degrees before the compressor and subcooling before the expansion process. HCFO-1233zd(E) was chosen as an example to demonstrate the various thermodynamic states due to its favourable thermodynamic and environmental properties and A1 safety classification.

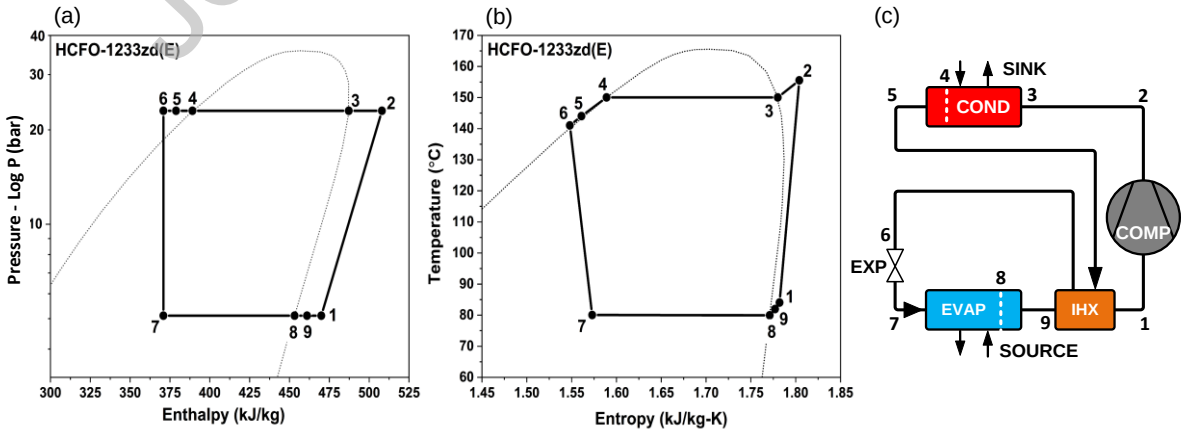

Fig. 3. Presents (a) Log P-h diagram for HCFO-1233zd(E), (b) T-s diagram for HCFO-1233zd(E), and (c) schematic with state points representing a HTHP cycle with IHX.

3.1 Simulation model

The cycle modelling was subjected to the following specific assumptions,

- Steady-state conditions
- Discharge and suction temperatures varied according to the required minimum superheat
- Potential and kinetic energy was neglected
- Assumed heating capacity 11 kW (matched to laboratory scale experimental testing)
- Electromechanical efficiency assumed to be 0.95, and ambient temperature 295.15 K (T_0)
- Pressure drops along the heat exchangers and pipelines was neglected
- Heat dissipation to the surroundings was neglected
- Isenthalpic expansion valve process, $h_6 = h_7$
- Constant pinch temperatures in the evaporator ΔT_{evap} = 3 K and condenser ΔT_{cond} = 5 K
- IHX subcooling of 5 K.

The single-stage HTHP thermodynamic cycle was modelled to achieve heat sink temperatures up to 140 °C, integrating an IHX to improve energetic and exergetic efficiency and to support dry compression. The refrigerants HFC-245fa and HFC-365mfc were compared with low GWP refrigerants listed in Table 1 to determine the energy, exergy, and minimum superheat outputs. The temperature setpoints were T_{source} 60 and 70 °C, T_{sink} 90 and 140 °C, with T_{lift} at 30 and 70 K, Eqs. (1) to (5) were used to calculate energy and exergy within the system (Dincer & Rosen, 2015).

$$COP_{theo} = \frac{h_2 - h_5}{h_2 - h_1} \tag{1}$$

$$VHC = \rho_1 (h_2 - h_5) \tag{2}$$

$$Ex_{flow} = (h - h_0) - T_0(s - s_0) \tag{3}$$

$$Ex_{total} = Ex_{comp} + Ex_{cond} + Ex_{exp} + Ex_{evap} + Ex_{IHX} \tag{4}$$

$$\eta_{ex} = \left(1 - \left(\frac{Ex_{total}}{P_{comp}}\right)\right) x100 \tag{5}$$

In Eq. (6) and (7), Pierre's correlations were used to estimate the volumetric and global compression efficiencies as a function of the compression process pressure ratio. These equations are applicable for open compressors, overhanging refrigerant types, and a power range from 1 to 100 kW (Da Riva & Del Col, 2011). The correlation coefficients for the variables (k_1, k_2, k_s, k_e, a, & b) have respective values of (1.04, -0.066, 0.15, -0.1, -2.28, & 2.67) (Granryd, 2005). The IHX effectiveness was computed using Eq. (8) rather than assumed. The discharge temperature for all refrigerants was kept below the critical temperature by controlling the degree of superheat required to ensure dry compression in the compressor and regulate discharge temperature.

$$\eta_{vol} = k_1 \left(1 + \frac{T_{suc} - 18}{100} * k_s\right) \exp^{\left(\frac{P_{dis}}{P_{suc}} * k_2\right)} \tag{6}$$

$$\frac{\eta_{vol}}{\eta_{Global}} = 1.1 \left(1 + \frac{T_{suc} - 18}{100} * k_e\right) \exp^{\left(a * \frac{T_{cond}}{T_{evap}} + b\right)} \tag{7}$$

$$\varepsilon_{IHX} = \frac{h_1 - h_9}{h_5 - h_9} \tag{8}$$

4. Minimum superheat

Alongside the refrigerant's thermophysical properties, the behaviour throughout the isentropic compression process in the HTHP cycle was mainly determined by the working fluid's saturation vapour shape at high entropy values. Based on the saturated vapour slope T-s diagram shown in Fig. 4, refrigerants used in the vapour compression cycle are categorised into different types: dry, isentropic, or wet. The criteria used to define these refrigerants characterise a positive slope as dT/ds >0 (dry), a negative slope as dT/ds <0 (wet) or an infinite slope as dT/ds ≅0 (isentropic) (Granryd, 2005; Bao & Zhao, 2013). Refrigerants with a re-entrant saturated vapour line are usually described as overhanging or extremely overhanging, depending on the severity of the slope.

An effective method is to differentiate the slope and determine the angle of the vapour slope, as shown in Fig. 4 for HCFC-22, HFO-1234ze(Z), and HC-600. The HCFC (hydro chlorofluorocarbon) R22, although no longer produced and in the process of phasing out of use, is referenced as an example of a wet refrigerant type to show variation within the graph. Isentropic refrigerants have an angle of approximately 90°, wet refrigerants <90°, and dry refrigerants >90° (Reißner , 2015). In addition, the molecular degree of freedom and the molecular weight are other methods to determine the type of slope (Su, et al., 2017). According to Tabor & Bronicki (1965) molecules with a small number of atoms are described as wet, whereas dry refrigerants have a larger number of atoms and an isentropic shape with an atomic number between 5 to 10.

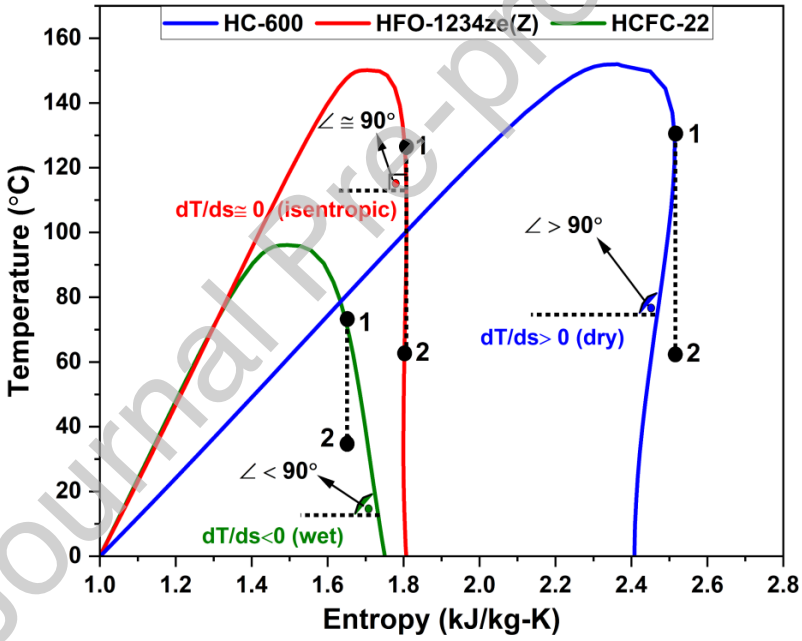

Fig. 4. Refrigerant type classification based on saturated vapour slope characteristics.

In this work, an assessment was completed of the minimum superheat degree required at the compressor for the selected refrigerants shown in Table 1. The refrigerant HFO-1234ze(Z) is isentropic and has a negligible superheat requirement of ≤ 5 K for dry compression. For re-entrant shapes (e.g., HCFO-1233zd(E) or HFO-1336mzz(Z)), the maximum saturation point was determined at vapour quality (x=1) and temperatures ranging between 60 and 130 °C, as shown in Fig. 5; at these parameters' entropy remains constant with suction temperature determined using Eq. (9) and Eq. (10).

$$s_1 = f(T = 125\ °C, x = 1) \tag{9}$$

$$T_1 = f(s_1, P_{evap}) \tag{10}$$

In the case of extremely overhanging refrigerants like HFC-365mfc and HFO-1336mzz(Z), the entropy saturation pressures at the evaporator and condenser were used to calculate the minimum degree of superheat required at the compressor. The suction entropy formula Eq. (11) was developed using the T-s diagram (see Fig. 5), considering an adjustable factor F_{adj} to ensure dry compression and compressor discharge temperature 5 to 10 K higher than the condensation temperature. Keeping the discharge temperature within a range of 5 to 10 K above condensation temperature for the subcritical technique will minimise the power input of the compressor and provide a steady heat at a specific condensation temperature below the critical temperature of the working fluid, thereby covering a more comprehensive range of industrial processes. In addition, the suction temperature is a function of suction entropy and evaporation pressure Eq. (12). The necessary degree of superheat required was calculated using Eq. (13), which calculates the differential between suction and evaporation temperatures at the maximum point on the vapour curve slope.

$$s_{suc} = (s_2 - s_1)F_{adj} + s_1 \tag{11}$$

$$T_{suc} = f(s_{suc}, P_{sat,evap}) \tag{12}$$

$$T_{SH} = T_{suc} - T_{evap} \tag{13}$$

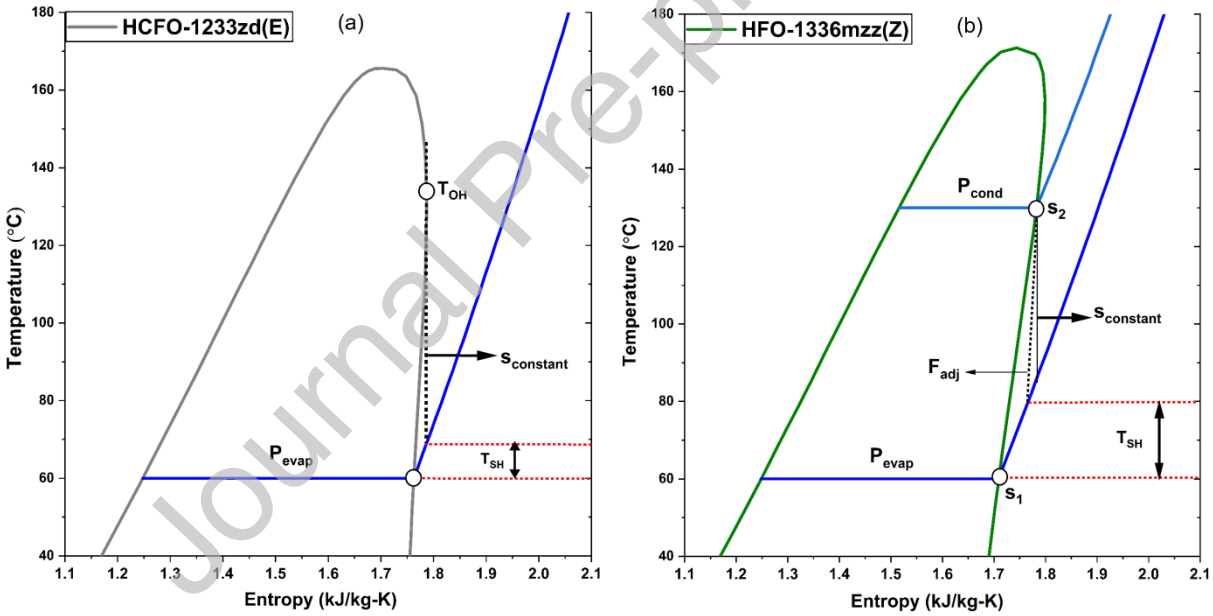

Fig. 5. Graphs showing the temperature as a function of entropy, with additional lines outlining the calculation approach to determine requisite superheat for each refrigerant; (a) HCFO-1233zd(E) (overhanging), and (b) HFO-1336mzz(Z) (extremely overhanging) (Adapted from Sulaiman, et al., (2022)).

5. Results and discussion

The following section presents and discusses the energetic and exergetic performance results of the subcritical HTHP system at various heat source and heat sink temperatures and provides a practical method to map the minimum superheat at the compressor for the refrigerants investigated.

5.1 Energetic performance

Table 2 shows the energetic and exergetic performance results for the refrigerants investigated. The data reveals the relationship between the condensation line to the dome of the log(p)-h diagram and COP. As the condensation line moves towards the critical temperature, it reduces the COP for all refrigerants because the distance between the saturation vapour and the liquid line becomes smaller when approaching the critical point, resulting in a shorter condensation line and a smaller enthalpic difference at the condenser. Furthermore, the decrement in the de-superheat area between the discharge point and saturation vapour line occurs due to the overhanging profile of each refrigerant.

The optimum value of COP for the refrigerants with an overhanging shape is achieved at T_{cond} = 130 °C with reduced performance at higher or lower condensation temperatures. Unlike the VHC, which is a function of the suction density and change in enthalpy at the condenser between inlet and outlet points, the VHC increases at higher evaporation and condensation temperatures due to increased suction density. Apart from HFO-1234ze(Z), the discharge temperature is less than 10 °C above the condensation temperature for all refrigerants based on the input parameters, assumptions, and minimum superheat required in each case. Compared to HFC-245fa and HFC-365mfc, a trade-off between COP, VHC, and exergetic efficiency is necessary to select the most suitable working fluid in HTHP applications.

Table 2: HTHP theoretical energetic and exergetic results at different evaporation and condensing setpoints.

	$(T_{evap} = 60\ ℃ \& T_{cond} = 90\ ℃, 130\ ℃)$						$(T_{evap} = 70\ ℃ \& T_{cond} = 100\ ℃, 140\ ℃)$					
Refrigerant	T_{dis} (℃)	**COP [-]**	**VHC** $(kJ.m^{-3})$	W_{in} (kW)	Ex_{dest} (kW)	η_{ex} (%)	T_{dis} (℃)	**COP [-]**	**VHC** $(kJ.m^{-3})$	W_{in} (kW)	Ex_{dest} (kW)	η_{ex} (%)
R1233zd(E)	95.97	7.93	3316	1.93	1.03	62.50	104.30	7.82	4110	1.89	1.03	61.81
	137.30	3.08	2633	5.87	3.80	49.59	145.90	3.04	3105	5.81	3.74	47.80
R245fa	95.52	7.76	3925	1.98	1.06	61.10	103.90	7.58	4873	1.95	1.03	60.17
	134.90	2.83	2876	6.47	4.33	45.54	144.00	2.71	3288	6.54	4.40	42.77
R1336mzz(Z)	93.41	7.99	2273	1.95	1.04	62.45	103.50	7.86	2886	1.89	1.01	62.18
	140.90	3.13	1854	6.07	3.91	49.91	148.60	3.09	2203	5.88	3.66	48.75
R365mfc	93.56	8.09	1899	1.95	1.06	62.63	103.10	8.00	2439	1.89	1.01	62.52
	141.70	3.18	1566	6.08	3.96	50.75	149.40	3.14	1948	5.78	3.61	50.37
R1224yd(Z)	95.52	8.14	3602	1.95	1.03	61.71	103.70	8.1	4426	1.92	1.00	60.68
	134.70	2.92	2678	6.23	4.10	46.50	144.00	2.89	3061	6.32	4.18	43.77
R600	95.20	7.62	4633	1.94	1.01	61.66	103.40	7.61	5540	1.92	0.99	60.37
	133.70	2.80	3378	6.00	3.86	46.38	143.50	2.78	3692	6.27	4.13	42.67
R601	93.71	8.28	1935	1.90	1.02	63.70	103.5	8.16	2433	1.85	0.98	63.30
	141.40	3.31	1623	5.54	3.46	53.30	154.01	3.23	1991	5.32	3.20	52.80
R1234ze(Z)	98.24	7.88	3221	1.94	1.08	61.91	107.80	7.75	5177	1.91	1.05	61.02
	142.90	3.02	3174	4.74	4.02	47.88	152.40	3.00	3589	6.12	4.09	45.07

Fig. 6 (a) presents the relationship between the pressure ratio and the compressor's input power (W_{in}) for the selected refrigerants at temperature lifts between 30 K and 70K. At a temperature lift of 70 K, the pressure ratio ranges from 3.8 to 5.3, and the input power of the compressor is between 5.5 and 6.6 kW. With HFC-245fa displaying the highest compressor input power and HC-601 the lowest, HC-600 had the lowest value for pressure ratio and HFC-365mfc the highest. The data shows that refrigerants with increasing values of saturated vapour slope (re-entrant to extremely re-entrant) tend to have higher pressure ratios and lower compressor input power.

Fig. 6 (b) illustrates the trade-off between COP and VHC for the investigated refrigerants. There is a direct relationship between temperature lift and the energetic performance of the HTHP system, with lower temperature lift resulting in higher COP and VHC for all refrigerants. At 30 and 70 K temperature lift, HC-600 and HFO-1234ze(Z) show the highest VHC values, whereas HC-601 has the lowest. HFC-245fa shows the lowest COP value at different temperature lifts, and HC-601 is the highest.

Compared to HFC-245fa, refrigerant HCFO-1233zd(E) has a COP of 2% to 3% higher at T_{cond} = 130 °C and 140 °C at T_{lift} = 30 K, increasing to 12% at T_{lift} = 70 K at similar heat sink temperatures. This is because HCFO-1233zd(E) possesses a higher critical temperature and, therefore, a longer condensation line. As a result of its higher suction density value, HFC-245fa shows a VHC value approximately 15% higher than HCFO-1233zd(E) at T_{lift} = 30 K, and this percentage is greatly reduced with increased temperature lift.

HC-601 provides the highest COP value amongst the candidates due to its favourable thermodynamic properties, including very high critical temperature. However, as it has a low VHC, this would require larger equipment within the system design.

HFO-1234ze(Z) exhibits good COP and a high VHC. However, the discharge temperature of HFO-1234ze(Z) is more than 10 K higher than the condensation temperature, which would limit its industrial application range. This is because HFO-1234ze(Z) has a higher isentropic component value than most refrigerants studied. In addition, HFO-1234ze(Z) has an isentropic refrigerant type in which the superheat occurs in the evaporator compared to HFC-365mfc, HFO-1336mzz(Z), and HC-601, requiring significantly lower superheat levels prior to the compressor.

HFO-1224yd(Z) has the second highest COP value at T_{lift} = 30 K, and this value rapidly falls at T_{lift} = 70 K due to increased input power required at high-temperature lift compared to other candidates.

HFO-1336mzz(Z), which is the most likely replacement for HFC-365mfc, showed a COP value of 3.1 at T_{cond} = 140 °C and T_{lift} = 70 K. Compared to HFC-365mfc, refrigerant HFO-1336mzz(Z) at T_{lift} = 70 K exhibits a 17% higher VHC at T_{cond} = 130 °C, and 15% at T_{cond} = 140 °C.

HCFO-1233zd(E) shows a good trade-off between variables COP, VHC and exergetic efficiency. HCFO-1233zd(E) at T_{evap} = 60 °C and T_{cond} = 130 °C exhibited a COP value of 3.14, VHC of 2633 kJ/m^3 and exergetic efficiency (η_{ex}) of 59%. HFO-1336mzz(Z) presented a similar COP value but a lower VHC of 1809 kJ/m^3 and lower exergetic efficiency of 52%. At different condensation temperatures, refrigerants HCFO-1233zd(E) and HFC-245fa required a minimum superheat temperature between 5 to 8 K, whereas HFO-1336mzz(Z) and HFC-365mfc required a value between 19 to 21 K at T_{lift} = 70 K.

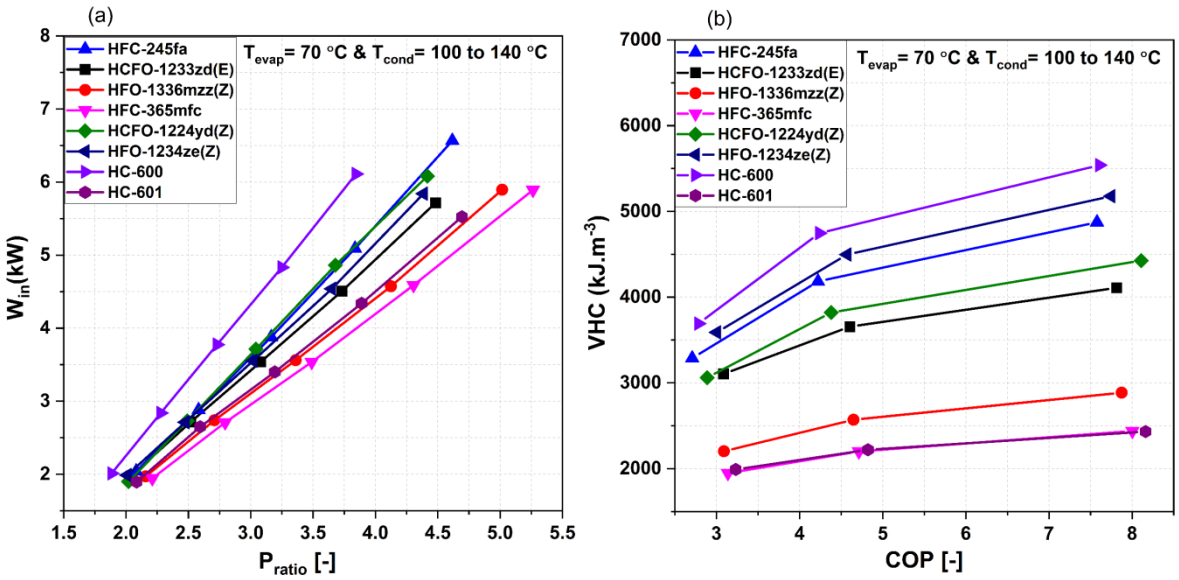

Fig. 6. (a) The estimated work done by the compressor as a function of pressure ratio at T_{lift} at 30 to 70 K; (b) The estimated VHC as a function of COP at T_{lift} at 30, 50 and 70 K exergetic analysis.

The exergy analysis is useful to define the quality of mechanical and thermal losses and, therefore, the potential energetic improvements to conserve energy. Fig. 7 presents the estimated exergy efficiency (η_{ex}) and the total exergy destruction (Ex_{des}) of each component and refrigerant.

The compressor has the highest exergetic loss compared to other components, ranging from 65% to 80%, with the expansion valve second highest, ranging from 7% to 22%. In addition, the condenser and evaporator show the lowest exergy destruction as they are not a function of the temperature lift. Further, the expansion valve exhibits low exergy destruction at low-temperature lift, related to an elevation in dissipative forces because of the high-pressure ratio.

At T_{lift} = 70 K, the results highlight HC-601 and HFC-365mfc as the most exergetic refrigerants, whereas HFC-245fa and HC-600 show the lowest. The exergy destruction of HFC-245fa is high compared to other candidates, and exergy destruction of the system increases at higher temperature lift. Furthermore, according to the exergy findings at T_{lift} = 40 K, the exergy efficiency does not drop appreciably compared to 50, 60, and 70 K.

The analysis also shows that increasing the evaporation temperature results in lower exergy efficiency within the system. Based on these results, mapping and controlling the minimum superheat could enable the system to achieve maximum exergetic efficiency while minimising losses from each key component in the heat pump cycle (i.e., compressor, condenser, evaporator, expansion valve and IHX).

(a) (b)

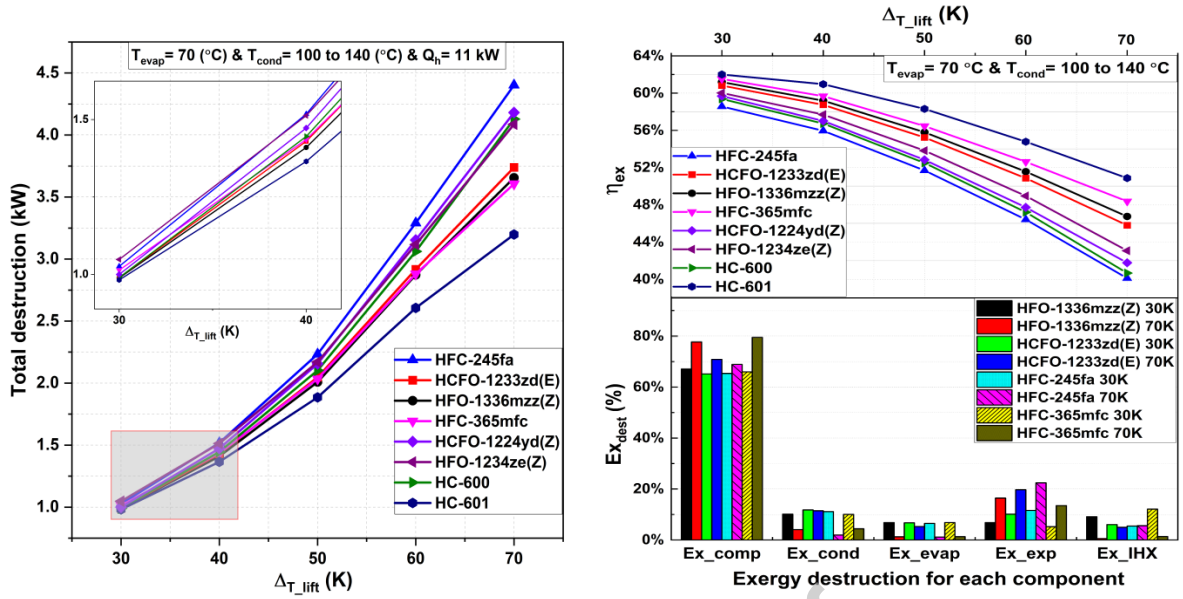

Fig. 7. (a) Plots the total exergy destruction as a function of temperature lift; (b) Comparison of the estimated % exergy destruction for each of the key components in the HTHP system and % exergy efficiency at different temperature lifts.

5.2 Mapping of the minimal superheat

The discharge temperature in a HTHP system plays an important role in achieving increased COP. The optimum practical method to control discharge temperature involves mapping the superheat degrees required by the compressor for each refrigerant, as shown in Fig. 8 (a). In this investigation, the minimum superheat is identified in Fig. 3 between the evaporator saturation line (point 8) and the compressor inlet (point 1). Alongside the compressor isentropic efficiency, the working fluid isentropic exponent (Cp/Cv) (see Table 1) at atmospheric pressure and temperature represents a significant factor in predicting the discharge temperature at the outlet of the compressor. As the isentropic value of the working fluid increases, it produces a higher discharge temperature.

According to numerical results, as T_{lift} increases, the minimal superheat T_{SH} required by the compressor also increases. The refrigerants HCFO-1233zd(E), HFC-245fa, HC-600, and HCFO-1224yd(Z) require T_{SH} <10 K above the evaporation temperature to the compressor suction inlet. Whereas HFO-1336mzz(Z), HC-601 and HFC-365mfc required $T_{SH} \geq 18$ K at T_{lift} = 70 K. The results indicate that the suction and discharge pressures and system temperature lift influence each refrigerant's required minimum degree of superheat.

Fig. 8 (b, c, d) depicts 3D contour plots of the required superheat degrees by the compressor for the three most promising refrigerant candidates (i.e., HCFO-1233zd(E), HFO-1336mzz(Z), and HCFO-1224yd(Z)). By mapping the optimal degree of superheat required at the compressor, the COP and VHC findings are in good agreement with the theoretical results reported by Arpagaus & Bertsch, (2019) with an improvement of up to 0.5% at T_{lift} = 70 K. Furthermore, overhanging refrigerants like HCFO-1233zd(E) will have a reduced heat exchange surface area compared to extremely overhanging refrigerants due to higher heat transfer coefficient values during condensation and evaporation processes.

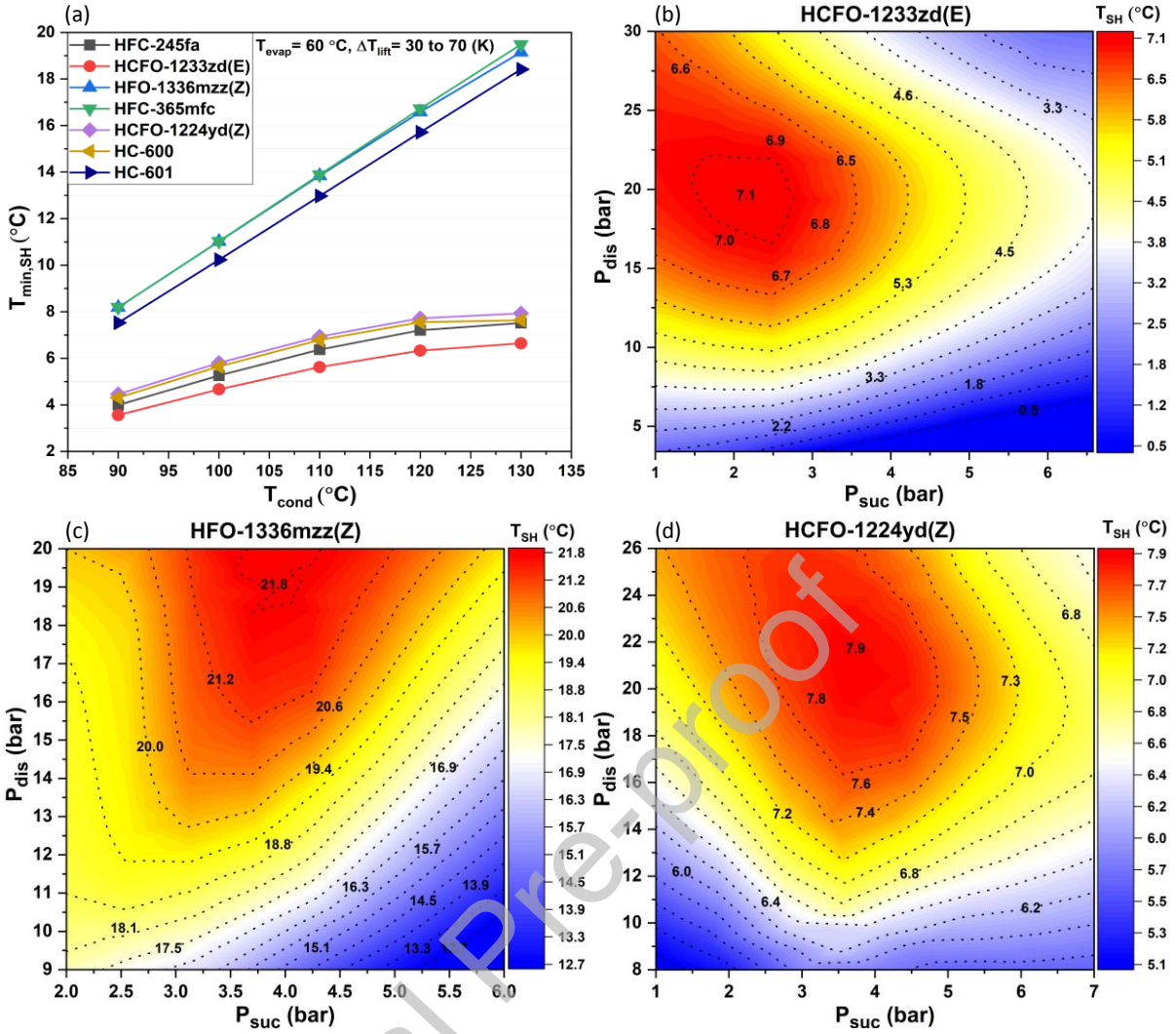

Fig. 8. (a) The minimal superheat degree for selected refrigerants at setpoints T_{evap} = 50 to 70 °C and T_{cond} = 90 to 130 °C and T_{lift} =30 to 70 K; (b, c & d) Contour plots of minimal superheat degree as a function of discharge pressure and suction pressure for HFO-1233zd(E), HFO-1336mzz(Z) and HCFO-1224yd(Z).

5.3 Model validation

The accuracy of the numerical simulations with the HTHP model was validated by comparing experimental COP results based on their conformance with statistical indices within permissible tolerance levels. In addition, experimental results from Arpagaus & Bertsch, (2019) of a single-stage HTHP with IHX were applied to verify the simulation results, which included nine experimental runs for each of the refrigerants, HCFO-1233zd(E), HCFO-1224yd(Z), and HFO-1336mzz(Z). The simulated results were compared with the experimental data at 40 to 80 °C heat source and 90 to 150 °C heat sink temperatures.

Furthermore, three statistical indices were utilised to validate and evaluate the reliability of simulation results: Percentage error (%Error), coefficient of determination (R^2), and root mean square error (RMSE). The equations Eq. (14, 15 & 16) describe the mathematical definitions for the three statistical indices.

$$\%\text{Error} = \left(\frac{Y_{Num} - Y_{Exp}}{Y_{Exp}}\right) \times 100 \qquad (14)$$

$$R^2 = \frac{\sum_{j=1}^{n}\left(Y_{Num} - \overline{Y}_{Exp}\right)}{\sum_{j=1}^{n}\left(Y_{Exp} - \overline{Y}_{Exp}\right)} \quad (15)$$

$$RMSE = \sqrt{\frac{\sum_{i=0}^{n}\left(Y_{Exp} - Y_{Num}\right)^2}{n}} \quad (16)$$

Note: Where, Y_{Num} are the numerical values, Y_{Exp} the experimental values, $\overline{Y}_{Exp}$ the average experimental values and n is the number of reference data.

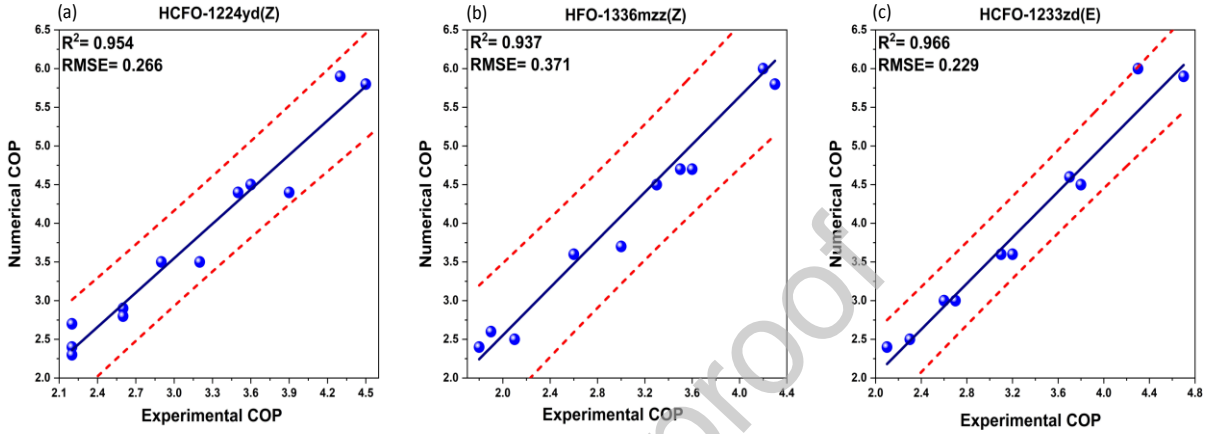

Fig. 9. Validation of the numerical and experimental COP for the main three investigated refrigerants, (a) HCFO-R1224yd(Z), (b) HFO-1336mzz(Z), and (c) HCFO-1233zd(E) under various heat source and heat sink temperature parameters.

In Fig. 9, the statistical results show that the coefficients of determination R^2 of COP for HCFO-1233zd(E), HCFO-1224yd(Z), and HFO-1336mzz(Z), respectively, are 0.966, 0.954, and 0.937. Furthermore, the statistical analysis reveals a close regression line to the experimental points, indicating that the analysed simulated COP agrees with the empirical values and that the HTHP model is reliable for future predictions.

In contrast, the standard error (SE) between the numerical and empirical COP for HFO-1336mzz(Z), HCFO-1233zd(E), and HCFO-1224yd(Z) lies between 13% to 42%, 8% to 27%, and 9% to 32%, respectively. These relatively high values of RMSE and SE result from the discrepancy between calculated and experimental values for the compressor discharge point. The HTHP system's actual COP highly depends on the discharge temperature and thermophysical characteristics. Furthermore, in the HTHP experimental tests, the system heat losses to the surroundings were estimated at about 21 ± 7%.

For all experimental data provided for validation, the discharge temperature was 30 K higher than the condensation temperature, resulting in a reduction in compressor isentropic efficiency, an increase in compressor input power, and, consequently, lower COP. In addition, at heat sink temperatures of 140 °C and 150 °C, the discharge temperature for the investigated refrigerants exceeded the critical temperature and was found in the supercritical zone, resulting in a COP that is substantially lower than the numerical COP.

In direct comparison, the numerical model was developed by mapping the superheat degrees required by the compressor for refrigerants that are overhanging and extremely overhanging. Mapping the appropriate superheat maintains the discharge temperature to no more than 10 K above the condensation temperature, resulting in lower input power and higher numerical COP compared to experimental COP.

6. Conclusions

A theoretical simulation model of a single-stage HTHP cycle incorporating an IHX was developed to investigate performance characteristics and optimisation methods for a range of suitable low GWP refrigerants. The main findings observed from this study are as follows:

- The assessment of the thermophysical and environmental properties yielded a limited number of potential low GWP refrigerant candidates (i.e., HC-600, HC-601, HCFO-1224yd(Z), HCFO-1233zd(E), HFO-1234ze(Z), and HFO-1336mzz(Z)) as replacements for HFC-245fa and HFC-365mfc in HTHP applications.
- Based on the energetic and exergetic performance results for the refrigerants investigated, a trade-off between COP, VHC, and exergetic efficiency is necessary to select the most suitable and promising working fluid. Therefore, the findings suggest the synthetic HCFO-1233zd(E) as a potential replacement for HFC-245fa and HFO-1336mzz(Z) for HFC-365mfc.
- Mapping the minimum superheat required by each refrigerant revealed a minimum superheat of <10 K for HCFO-1233zd(E), HFC-245fa, HC-600, HCFO-1224yd(Z), and a minimum superheat of ≥18 K for HFO-1336mzz(Z), HC-601, and HFC-365mfc at a T_{lift} = 70 K.
- Exergy analysis showed a considerable improvement in energetic and exergetic efficiency through mapping the minimum superheat for each refrigerant and potentially offering control parameters at heat source and heat sink loops. Due to their considerable exergy losses, the compressor and expansion valve was identified as the principal components for future performance improvement.
- Experimental validation of the simulation model based on three statistical indices verified that numerical COP values are consistent with observed experimental COP values. The high standard error and RMSE values indicated the need to map minimum superheat to optimise system setup and control within experimental activities.

Acknowledgements

The authors gratefully acknowledge the support from the Department for the Economy (Northern Ireland, EP/T022981/1) DEcarbonisation of Low TemperAture Process Heat Industry, DELTA PHI and EP/R045496/1 Low Temperature Heat Recovery and Distribution Network Technologies (LoT-NET).

In addition, the financial support of the Swiss Federal Office of Energy SFOE as part of the SWEET (SWiss Energy research for the Energy Transition) project DeCarbCH (www.sweet-decarb.ch) and the project Annex 58 HTHP-CH (Contract number SI/502336-01) are gratefully acknowledged.

References

AMOLEA, 2023. AMOLEA™ 1224yd. [Online]
Available at: https://www.agc-chemicals.com/file.jsp?id=30728
[Accessed 03 01 2023].

Arpagaus, C. & Bertsch, S. S., 2019. Experimental results of HFO/HCFO refrigerants in a laboratory scale HTHP with up to 150 °C supply temperature. Copenhagen, s.n.

Arpagaus, C. & Bertsch, S. S., 2020. Experimental comparison of HCFO R1233zd(E) and R1224yd(Z) in a high temperature heat pump up to 150 °C. Glasgow, s.n.

Arpagaus, C., Bless, F. & Bertsch, S. S., 2020. Theoretical Analysis of Transcritical HTHP Cycles with Low GWP - Paper ID: 1168. Glasgow, Institute of Refrigeration.

Arpagaus, C. et al., 2018. High temperature heat pump using HFO and HCFO refrigerants - System design, simulation, and first experimental results. Purdue, International Refrigeration and Air Conditioning Conference.

Arpagaus, C. et al., 2018. High temperature heat pumps: Market overview, state of the art, research status, refrigerants, and application potentials. Energy, Volume 152, pp. 985-1010.

ASHRAE, 2022. ANSI/ASHRAE Standard 34-2022- Designation and Safety Classification of Refrigerants. [Online]
Available at: https://www.ashrae.org/technical-resources/standards-and-guidelines/ashrae-refrigerant-designations
[Accessed 29 12 2022].

Bamigbetan, O. et al., 2018. Theoretical analysis of suitable fluids for high temperature heat pumps up to 125 °C heat delivery. International Journal of Refrigeration, Volume 92, pp. 185-195.

Bamigbetan, O. et al., 2019. Experimental Investigation of a prototype R-600 Compressor for High Temperature Heat Pump. Energy, Volume 169, pp. 730-738.

Bao, J. & Zhao, L., 2013. A review of working fluid and expander selections for organic Rankine cycle. Renewable and Sustainable Energy Reviews, Volume 24, pp. 325-342.

Besagni, G., Mereu, R., Di Leo, G. & Inzoli, F., 2015. A study of working fluids for heat driven ejector refrigeration using lumped parameter models. International Journal of Refrigeration, Volume 58, pp. 154-171.

Bianchi, G. et al., 2019. Estimating the waste heat recovery in the European Union. Energy, Ecology and Environment, 4(5), pp. 211-221.

Da Riva, E. & Del Col, D., 2011. Performance of a semi-hermetic reciprocating compressor with propane and mineral oil. International Journal of Refrigeration, 34(3), pp. 752-763.

DEFRA, 2022. Assessment of the F gas Regulation in Great Britain. [Online]
Available at: https://www.gov.uk/government/publications/assessment-of-the-f-gas-regulation-in-great-britain
[Accessed 03 01 2023].

Dincer, I. & Rosen, M. A., 2015. Exergy Analysis of Heating, Refrigerating and Air Conditioning: Methods and Applications. s.l.:Academic Press.

EEA, 2021. EEA greenhouse gases - data viewer. [Online]
Available at: https://www.eea.europa.eu/data-and-maps/data/data-viewers/greenhouse-gases-viewer
[Accessed 02 09 2022].

EUR-Lex, 2014. Regulation (EU) No 517/2014 of the European Parliament and of the Council of 16 April 2014 on fluorinated greenhouse gases and repealing Regulation (EC) No 842/2006. [Online] Available at: http://data.europa.eu/eli/reg/2014/517/oj
[Accessed 04 01 2023].

Eyerer, S. et al., 2019. Experimental investigation of modern ORC working fluids R1224yd(Z) and R1233zd(E) as replacements for R245fa. Applied Energy, Volume 240, pp. 946-963.

Forman, C., Muritala, I. K., Pardemann, R. & Meyer, B., 2016. Estimating the global waste heat potential. Renewable and Sustainable Energy Reviews, Volume 57, pp. 1568-1579.

Fukuda, S., Kondou, C., Takata, N. & Koyama, S., 2014. Low GWP refrigerants R1234ze(E) and R1234ze(Z) for high temperature heat pumps. International Journal of Refrigeration, Volume 40, pp. 161-173.

Granryd, E., 2005. Refrigeration Engineering. s.l.:Royal Institute of Technology-Department of Energy Technology.

Honeywell , 2023. A Better Environment with Next-Generation Solstice® zd Refrigerant. [Online] Available at: https://www.honeywell-refrigerants.com/europe/wp-content/uploads/2018/11/Honeywell-Solstice-zd-Brochure_EN.pdf
[Accessed 03 01 2023].

IEA HPT, 2023. Annex 58: Task 1: Technologies – State of the art and ongoing developments for systems and components. [Online]
Available at: https://heatpumpingtechnologies.org/annex58/task1/
[Accessed 03 02 2023].

IEA, 2022. World total final consumption by source, 1971-2019. [Online]
Available at: https://www.iea.org/data-and-statistics/charts/world-total-final-consumption-by-source-1971-2019
[Accessed 02 11 2022].

Klein, S., 2017. Engineering Equation Solver (EES) V10.268, Madison. USA: Fchart software.

Kontomaris, K., 2014. HFO-1336mzz-Z: High Temperature Chemical Stability and Use as A Working Fluid in Organic Rankine Cycles. Purdue, s.n.

Mateu-Royo, C., Mota-Babiloni, A. & Navarro-Esbrí, J., 2021. Semi-empirical and environmental assessment of the low GWP refrigerant HCFO-1224yd(Z) to replace HFC-245fa in high temperature heat pumps. International Journal of Refrigeration, Volume 127, pp. 120-127.

Mateu-Royo, C. et al., 2019. Experimental exergy and energy analysis of a novel high-temperature heat pump with scroll compressor for waste heat recovery. Applied Energy, Volume 253, p. 113504.

Mikielewicz, D. & Wajs, J., 2019. Performance of the very high-temperature heat pump with low GWP working fluids. Energy, Volume 182, pp. 460-470.

Mujahid Rafique, M., Gandhidasan, P., Al-Hadhrami, L. M. & Rehman, S., 2016. Energy, Exergy and Anergy Analysis of a Solar Desiccant. Journal of Clean Energy Technologies, 4(1), pp. 78-83.

Myhre, G. et al., 2013. : Anthropogenic and Natural Radiative Forcing. In: Climate Change 2013: The Physical Science Basis. Contribution of Working Group I to the Fifth Assessment Report of the Intergovernmental Panel on Climate Change . Cambridge, United Kingdom and New York, NY, USA: Cambridge University Press, pp. 659-740.

NIST, 2018. REFPROP - NIST Reference Fluid Thermodynamic and Transport Properties Database (REFPROP): Version 10.0, Gaithersburg: Standard Reference Data, NIST.

Odyssee-Mure, 2019. Sectoral Profile - Overview - Final energy consumption by sector in EU. [Online]
Available at: https://www.odyssee-mure.eu/publications/efficiency-by-sector/overview/final-energy-consumption-by-sector.html
[Accessed 2023 12 27].

Ommen, T. et al., 2015. Technical and economic working domains of industrial heat pumps: Part 1 – Single stage vapour compression heat pumps. International Journal of Refrigeration, Volume 55, pp. 168-182.

Opteon, 2023. Opteon™ MZ. [Online]
Available at: https://www.opteon.com/en/-/media/files/opteon/opteon-mz-heat-transfer-fluid-technical-info.pdf?rev=2c7de628d3804f83a716dc94468b576d
[Accessed 03 01 2023].

Papapetrou, M. et al., 2016. Industrial waste heat: Estimation of the technically available resource in the EU per industrial sector, temperature level and country. Applied Thermal Engineering, Volume 138, pp. 207-216.

Patten, K. O. & Wuebbles, D. J., 2010. Atmospheric lifetimes and Ozone Depletion Potentials of trans-1-chloro-3,3,3-trifluoropropylene and trans-1,2-dichloroethylene in a three-dimensional model. Atmospheric Chemistry and Physics, Volume 10, pp. 10867-10874.

Petr, P. & Raabe, G., 2015. Evaluation of R-1234ze(Z) as drop-in replacement for R-245fa in Organic Rankine Cycles – From thermophysical properties to cycle performance. Energy, Volume 93, Part 1, pp. 266-274.

Reißner , F., 2015. Development of a Novel High Temperature Heat Pump System- Doctoral Thesis. Nürnberg: Friedrich-Alexander-Universität Erlangen-Nürnberg (FAU).

SOLKANE, 2023. SOLKANE-365/ Technical / Product Data Sheet (TDS/PDS). [Online]
Available at: https://www.solvay.com/en/product/solkane-365-mfc
[Accessed 03 01 2023].

Statista GmbH, 2022. Carbon dioxide emissions from energy worldwide from 1965 to 2021, by region. [Online]
Available at: https://www.statista.com/statistics/205966/world-carbon-dioxide-emissions-by-region/
[Accessed 02 09 2022].

Sulaiman, A. Y. et al., 2022. Thermodynamic analysis of subcritical High-Temperature heat pump using low GWP Refrigerants: A theoretical evaluation. Energy Conversion and Management, Volume 268, p. 116034.

Su, W., Zhao, L., Deng, S. & Zhao, Y., 2017. How to predict the vapor slope of temperature-entropy saturation boundary of working fluids from molecular groups?. Energy, Volume 135, pp. 14-22.

Tabor, H. & Bronicki, L., 1965. Establishing Criteria for Fluids for Small Vapor Turbines. SAE Transactions, Volume 73, pp. 561-575.

UNEP, 2020. Handbook for the Montreal Protocol on Substances that Deplete the Ozone Layer - Fourteenth edition. [Online]
Available at: https://ozone.unep.org/sites/default/files/Handbooks/MP-Handbook-2020-English.pdf
[Accessed 09 01 2022].

Worrella, E. & Biermans, G., 2005. Move over! Stock turnover, retrofit and industrial energy efficiency. Energy Policy, 33(7), pp. 949-962.

Statements and Declarations

The authors declare that they have no known competing financial interests or personal relationships that could have appeared to influence the work reported in this paper.

Signature: *Adam Sulaiman*